Deactivation of submelt laser annealed arsenic ultrashallow junctions in silicon during subsequent thermal treatment

Damiano Giubertoni[a] and Giancarlo Pepponi
Center for Materials and Microsystems—Irst—Fondazione Bruno Kessler, via Sommarive 18, Povo, Trento 38050, Italy

Mehmet Alper Sahiner
Department of Physics, Seton Hall University, South Orange, New Jersey 07079

Stephen P. Kelty
Department of Chemistry and Biochemistry, Center for Computational Research, Seton Hall University, South Orange, New Jersey 07079

Salvatore Gennaro and Massimo Bersani
Center for Materials and Microsystems—Irst—Fondazione Bruno Kessler, via Sommarive 18, Povo, Trento 38050, Italy

Max Kah and Karen J. Kirkby
Surrey Ion Beam Centre, Advanced Technology Institute, Faculty of Engineering and Physical Sciences, University of Surrey, Guildford GU2 7XH, United Kingdom

Roisin Doherty and Majeed A. Foad
Front End Products, Applied Materials Inc., 974 E. Arques Avenue, Sunnyvale, California 94085

F. Meirer and C. Streli
ATI, TU Wien, Stadionallee 2, 1020 Vienna, Austria

Joseph C. Woicik
National Institute of Standards and Technology, Gaithersburg, Maryland 20899

Piero Pianetta
SSRL/SLAC, 2575 Sand Hill Road, Menlo Park, California 94025

(Received 22 June 2009; accepted 8 September 2009; published 1 March 2010)

The use of nonequilibrium annealing approaches can produce very high levels of arsenic electrical activation in Si. However, subsequent thermal treatments between 500 and 800 °C easily deactivate the dopant to a level one order of magnitude below the solid solubility. In this work, the authors study the deactivation of laser annealed (LA) ultrashallow arsenic distributions in silicon using Hall effect measurements, extended x-ray absorption fine structure spectroscopy, and secondary ion mass spectrometry. Single crystal Si (100) wafers implanted with As ions at 2 keV energy and different doses were activated with a millisecond LA at 1300 °C using a scanning diode laser annealing system under nonmelt conditions. The samples were then thermally treated in a furnace at 300–900 °C in a N_2 atmosphere for 10 min. Electrical deactivation has been observed for all the implanted doses but for the lowest one. In particular, it was observed that the higher the As dose the easier the deactivation, in particular, after the 700 °C post-LA treatment. At 900 °C, in-depth diffusion and a resulting reactivation has been observed for samples implanted with 1×10^{15} and 3×10^{15} cm^{-2}. © *2010 American Vacuum Society.* [DOI: 10.1116/1.3242637]

I. INTRODUCTION

The need for ultrashallow junctions to realize source and drain extensions in Si complementary metal oxide semiconductor devices has resulted in the broad use of arsenic as the *n*-type dopant because of its low diffusivity and good solid solubility. In fact, a very high degree of dopant electrical activation is required because the sheet resistance of source and drain extensions has to be maintained at a low level. This may be produced exploiting nonequilibrium annealing approaches such as millisecond or nanosecond annealing (e.g., flash or laser annealing).[1] However, it is well known that when high concentrations of As ($>10^{20}$ cm^{-3}) are subjected to subsequent thermal treatments between 500 and 800 °C, the dopant is easily deactivated saturating at a level one order of magnitude below the solid solubility limit.[2–4] Several experimental results[4–7] and first principles calculations[8,9] suggested that the main mechanism behind this deactivation is the clustering of As atoms around vacancies forming As_nV defect and the injection of interstitials. More recent findings seem to suggest that defects involving self-interstitials may also play a relevant role, at least in some phases of the deactivation kinetics.[10,11]

In this work, the deactivation of laser (submelt) annealed ultrashallow arsenic distributions in silicon (2 keV ion implants) has been investigated. The combined use of Hall ef-

[a]Electronic mail: giuberto@fbk.eu

fect measurements, extended x-ray absorption fine structure spectroscopy (EXAFS), and secondary ion mass spectrometry (SIMS) gave an insight into the phenomenon when the dopant is confined in the first 10–20 nm of silicon.[12] Furthermore, the impact of the As concentration on the deactivation behavior was investigated by varying the implanted dose. A least-squares fit of the Fourier transform (FT) of the EXAFS function enabled us to obtain quantitative estimates of the As fractions in substitutional sites, clustered in As_nV defects, or precipitated in a SiAs monoclinic phase. These fractions when compared to the carrier concentrations obtained from Hall effect measurements helped understand the mechanisms behind the deactivation.

II. EXPERIMENT

Single crystal *p*-type Si (100) was implanted with As^+ ions at 2 keV energy (0° tilt). The implanted fluences were 1×10^{14}, 3×10^{14}, 1×10^{15}, and 3×10^{15} cm^{-2}, respectively. Ion damage was annealed and dopant activated with millisecond annealing at 1300 °C using a scanning diode laser annealing (LA) system under nonmelt conditions in a N_2 atmosphere. Both the ramp-up and ramp-down rates were of the order of 10^6 °C/s, whereas the sample was kept at the given temperature for 1 ms. The annealing temperature was monitored using a pyrometer calibrated through a NIST traceable standard. The laser power was controlled in order to ensure a stable temperature ±1 °C. Part of the LA annealed samples was then thermally treated in a furnace in an O_2/N_2 atmosphere for 10 min at 300, 500, 700, and 900 °C. A 1×10^{15} $cm^{-2}/100$ keV As implant laser (melting) annealed with a presumed high level of electrical activation was used as a reference for the EXAFS analyses.

The van der Pauw method was used to measure sheet resistance (R_s). The carrier dose and mobility values were determined using Hall effect measurements. An applied magnetic field of 0.328 T and Hall scattering factor of unity were used. SIMS analysis was carried out to obtain As depth profiles. A 0.5 keV (45° incidence) Cs^+ ion primary beam was used for collecting $^{28}Si^{75}As^-$ ions from a 66 μm diameter area centered in a 250×250 μm^2 rastered area.[13] Cross comparison with other complimentary techniques revealed an agreement in dose measurement within a 10% margin.[14]

EXAFS analysis was carried out either at the BM08 GILDA beamline of the European Synchrotron Radiation Facility or at beamline 10-2 of the Stanford Synchrotron Radiation Lightsource (SSRL) in grazing incidence and fluorescence acquisition with a side-looking 13 element GeHP detector. As *K*-edge spectra have been acquired in the energy range 11 600–12 700 eV with variable energy steps (0.5 eV near the edge, 5 eV at the scan periphery) at an incidence angle above the critical angle for total external reflection (about 0.18° measured from the sample surface) for all samples. The chosen angle of incidence allowed sampling of the whole dopant distribution with almost uniform weight across the implant. An iterative wet etch/oxidation process was carried out on the samples where an As accumulation peak was created at the surface SiO_2/Si interface (e.g., the LA+900 °C 10 min annealed samples as revealed by SIMS) in order to sample just the deeper part of the junction.[15]

Theoretical EXAFS functions were calculated using the University of Washington's multiple scattering XAFS calculation code FEFF8.4. Structural parameters obtained by the density functional theory (DFT) calculations (as explained below) for substitutional As in Si, As_nV clusters ($n\leqslant4$), and monoclinic SiAs precipitates were used for calculating the expected EXAFS functions $\chi(k)$. A least-squares fit of the FT of the $\chi(k)$ was carried out in order to quantify the fractions of As involved in the different aforementioned structures (the fits were carried out assuming the copresence of all the structures). The experimental EXAFS functions were extracted by subtracting the atomic absorption background using the AUTOBK code. The $\chi(k)$'s are then FT using a Gaussian window for (2.0–10.0 $Å^{-1}$) *k*-range with a k^2 weighting in order to fully account for the contribution from the larger *k* region. Details are reported elsewhere.[12] The geometry optimizations in the DFT calculations were carried out for four systems containing a Si vacancy surrounded by one to four As substitutional atoms using the CASTEP plane wave density functional code. Initial state structures of As_nV were prepared relaxing a bulk Si crystal (*Fd3m*) using the GGA PW-91 exchange-correlation functional to less than 0.01 eV/atom. The relaxed crystal was modified to contain a Si vacancy defect at the cell center and one to four As substitutional defects in the first coordination shell around the vacancy. Geometry optimizations of the defect states were carried out using fixed lattice parameters but flexible internal fractional coordinates in order to permit an optimization of the defect environment while retaining cubic bulk symmetry in the neighboring cells and bulk crystal lattice. The obtained lattice parameters and fractional displacements of the atoms in the first coordination shell around the vacancy are reported elsewhere.[12] In all cases, the vacancy neighbor shell atoms are displaced toward the vacancy on the order of 0.2–0.35 Å for As and 0.1–0.2 Å for Si.

III. RESULTS AND DISCUSSION

SIMS profiles obtained on the samples that were first laser annealed and then thermally treated in a furnace for 10 min at temperatures ranging from 300 to 900 °C are reported in Fig. 1. In order to compare the As diffusion in Si, the curves are plotted by aligning the interface between surface SiO_2 layer and Si substrate. In fact, after annealing in a partially oxidizing atmosphere, the SiO_2 layer growth increases with As concentration.[16] It is evident from SIMS that basically the LA treatment does not induce any relevant dopant indiffusion but only a slight redistribution between the surface and the projected range possibly due to solid phase epitaxial regrowth. The fact that variations of the junction depth (x_j) are not observed in those samples means that any possibly observed variation of R_s would be mainly due to variation in dopant activation and/or carrier mobility. In the 900 °C post-LA treatments two features are evident for all the im-

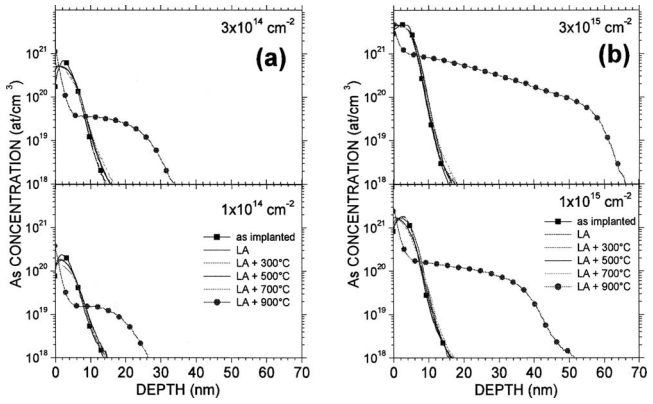

FIG. 1. Arsenic SIMS profiles obtained on the samples implanted with 2 keV As ions and doses of 1×10^{14} and 3×10^{14} cm^{-2} [(a) left] and 1×10^{15} and 3×10^{15} cm^{-2} [(b) right]. Curves aligned at the SiO_2/Si interface.

planted doses: an As peak accumulated at the SiO_2/Si interface and an accompanying diffusion with a dramatic increase in x_j.

Electrical characterization results are reported in Figs. 2 and 3 where the behavior of sheet resistance (R_s, van der Pauw) and active carrier areal concentration (Hall effect) are plotted versus the post-LA thermal treatment. The R_s values after only the LA step decrease with increasing As dose, from 1650 Ω/square for the 1×10^{14} cm^{-2} implanted sample to ~700 Ω/square for the 3×10^{15} cm^{-2} one. The latter has a R_s value quite similar to the one observed on the 1×10^{15} cm^{-2} sample (720 Ω/square) despite the three times larger implanted As dose. The R_s variation upon post-LA thermal treatment reveals two classes of behaviors depending on the As concentration: for the two lowest implanted doses the R_s is basically constant with a slight increase at 700–900 °C, whereas the highest doses at 700 °C reach a maximum and then decrease after the 900 °C, 10 min treatment. Finally, the R_s values measured on the etched samples are always twice those measured before the etching, supposedly because of the less retained dopant and the shallower junction.

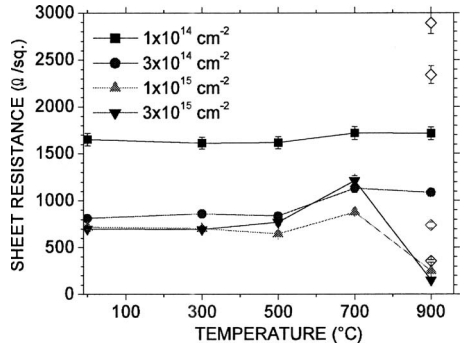

FIG. 2. Sheet resistance measured in van der Pauw geometry on the samples implanted at 2 keV with different As doses in function of the postlaser annealing 10 min thermal treatment. The hollow symbols at 900 °C refer to the etched samples.

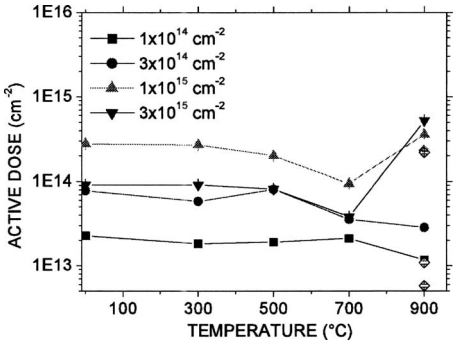

FIG. 3. Active carrier doses determined by Hall effect measurements on the samples implanted at 2 keV in function of the post-LA 10 min thermal treatment temperature. The hollow symbols at 900 °C refer to the etched samples.

The Hall effect measured active carrier dose values after the LA step always correspond to a 25%–30% fraction of the SIMS determined retained dose, but the highest dose (3×10^{15} cm^{-2}) has only an ~3.5% active dose corresponding to an absolute value lower than the one observed on the 1×10^{15} cm^{-2} sample and similar to that of the 3×10^{14} cm^{-2} implanted sample. The successive thermal treatment does not heavily affect the active carrier concentration for the two lowest doses apart from the 900 °C case that appreciably decreases it. For both sample series, the reduced active carrier concentration is partially compensated by the deeper x_j resulting in only a small increase in the measured R_s. The higher dose series shows a decrease in active carriers already at 500 °C and an even greater deactivation after the 700 °C step, whereas after the 900 °C it is evident a reactivation of the dopant has taken place. In particular, the 3×10^{15} cm^{-2} series always has lower values than the 1×10^{15} cm^{-2} series as observed after only the LA step. However, the situation is reversed once the LA step is followed by the 900 °C furnace anneal. A first interpretation of those results would suggest two different regimes depending on the actual As concentration present in the Si substrate. In fact, it is known that the active As concentration at equilibrium tends to saturate to a level an order of magnitude below the solid solubility limit. Nobili *et al.*[3] identified an expression for the actual equilibrium active carrier concentration for the 700–900 °C temperature range,

$$n_e = 2.2\times10^{22}\exp\left(-\frac{0.47}{kT}\right)\ \text{cm}^{-3}.$$

This means that at 700 °C the maximum active carrier concentration would be around 8×10^{19} cm^{-3}. A nonequilibrium annealing process such as laser annealing can create an active concentration higher than this limit, but the subsequent 10 min 700 °C treatment may decrease it toward the equilibrium value. This is actually what was observed in the samples implanted with the 1×10^{15} cm^{-2} dose or higher where the As concentration is far beyond the n_e value. In the lower doses, the As concentration is closer to the maximum active carrier density and less deactivation is expected. In order to verify if the mechanisms behind this deactivation

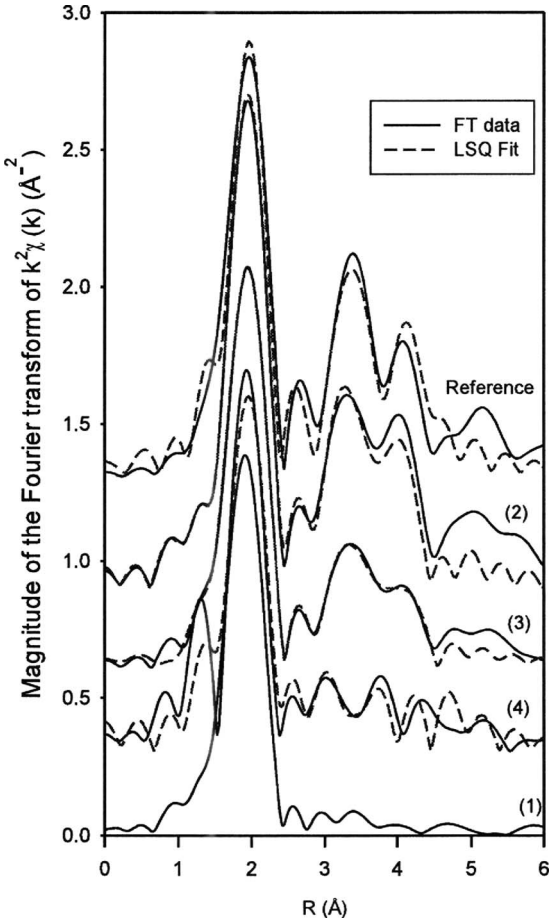

FIG. 4. Fourier transform of EXAFS functions and relative least-squares fits for samples: 1×10^{15} cm^{-2} as implanted (1), 3×10^{14} cm^{-2} LA (2), 1×10^{15} cm^{-2} LA (3), 3×10^{15} cm^{-2} LA (4), and the reference.

behavior are the same as observed for deeper As distributions reported in literature, e.g., the clustering of As around vacancies,[5] EXAFS analysis was carried out on selected samples.

Figure 4 reports the FT of the EXAFS $\chi(k)$ obtained from samples only subjected to LA together with the respective least-squares fits obtained from the simulations of the relaxed structures of As_nV defects obtained by DFT. These fits yielded an estimate of the fraction of As in substitutional lattice positions as reported in Table I: those values are in excellent agreement with the active As fraction, defined as the ratio between the Hall measured active carrier dose and the SIMS measured retained dose, for samples implanted with doses of 1×10^{15} cm^{-2} or higher. However, there is an appreciable discrepancy when comparing those values for the 3×10^{14} cm^{-2} implant, even considering the associated errors (4% for active carrier dose measured by Hall effect, 10% for SIMS dose). In this case, a comparison of the substitutional fraction from EXAFS and the active As fraction resulted in an apparent discrepancy of approximately 30%. This is currently under further investigation because an active fraction closer to the value obtained from EXAFS fits would be expected, given the concentration range for this sample. The fits permitted also an estimate of the amount of As involved in the different As_nV clusters and SiAs monoclinic precipitates (expected for concentrations beyond solid solubility). From these results, we can conclude that in the 3×10^{14} cm^{-2} case, the smaller deactivated fraction is mainly constituted by atoms in either AsV or As_3V structures. In the 1×10^{15} cm^{-2} sample, half of the As is expected to be inactive in As_3V clusters and 12% in AsV, whereas SiAs precipitates are not observed. The highest dose sample has a reduced population for the As_3V clusters, whereas 15% and 21% of As is in As_4V clusters and SiAs precipitates, respectively.

Finally, Fig. 5 shows the FT of EXAFS $\chi(k)$ measured on the 1×10^{15} cm^{-2} series (only qualitative data). As expected from the electrically active values, the FTs change very little up to 500 °C, whereas after the 700 °C treatment there is a reduction in the local order around the sampled As atoms as especially evidenced by the peaks related to the second neighbors (3–4 Å). However, after the 900 °C annealing the local order is partially recovered at least in the deeper part of the distribution as evidenced by the FT of the etched sample. This confirms that this thermal budget is able to break some of the As clusters and make the dopant indiffuse. Therefore, a higher fraction of arsenic is below the maximum active concentration and the junction depth is increased with the consequent reduction of the observed R_s values.

IV. CONCLUSION

A combined analytical approach has been applied to investigate the deactivation of As ultrashallow junctions real-

TABLE I. Active arsenic fraction (defined as the ratio between Hall-effect measured active carrier and SIMS-evaluated retained doses) and fractions of the As complexes from the least-squares EXAFS fits determined on the "only laser annealed" samples.

Sample ID	As dose (cm^{-2})	Hall/SIMS active fraction	Least-squares EXAFS fits					
			Subst. As	AsV	As_2V	As_3V	As_4V	SiAs
1	As impl.	⋯	⋯	⋯	⋯	⋯	⋯	⋯
2	3×10^{14}	0.27	0.44	0.11	0.04	0.30	0.08	0.03
3	1×10^{15}	0.27	0.26	0.12	0.02	0.53	0.05	0.00
4	3×10^{15}	0.03	0.05	0.16	0.05	0.38	0.15	0.21
Ref.	1×10^{15} (100 eV)	⋯	0.59	0.00	0.24	0.00	0.17	0.00

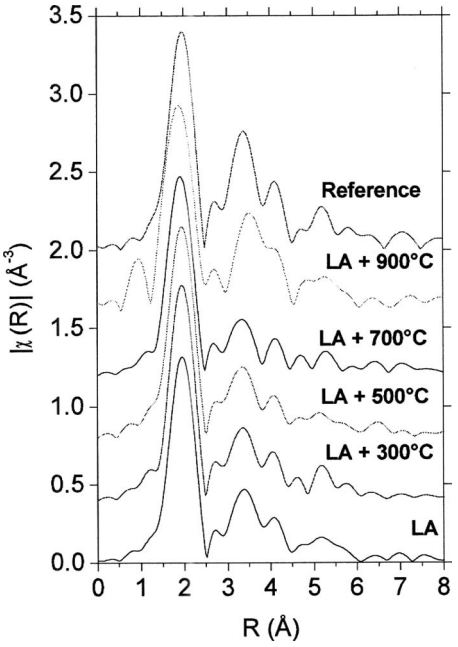

FIG. 5. Fourier transform of EXAFS functions for 1×10^{15} cm^{-2} implanted sample series. From the bottom: only laser annealed sample, LA+300 °C 10 min, LA+500 °C 10 min, LA+700 °C 10 min, LA+900 °C 10 min, and surface-etched reference. The curves are vertically shifted for clarity.

ized with 2 keV As^+ implants at different doses and then activated with a laser submelt process. Junction deactivation was induced by a 10 min thermal treatment in a furnace at temperatures ranging from 300 to 900 °C. Results indicated that the laser submelt process was able to activate in all cases only 25%–30% of the retained dose. However, in the case of the 3×10^{14} cm^{-2} sample, the substitutional fraction determined by the EXAFS fit would suggest a higher value, 44%, instead of the 27% expected from the Hall effect measurements. Successive thermal steps had a different impact depending on As concentration in Si. At the two lowest doses, the dopant activation is slightly affected by the temperature increase and a slight decrease in the activation is observed. On the other hand, for the two highest doses, As is strongly deactivated in the 500–700 °C window, and it is then reactivated with a 900 °C thermal treatment. The latter thermal treatment induces dramatic indiffusion and breaks the As_3V clusters which were identified by EXAFS as the primary deactivating defects for these ultrashallow systems. However, this 900 °C reactivation also results in a dramatic increase of the junction depth.

ACKNOWLEDGMENTS

The authors would like to acknowledge Francesco d'Acapito, INFM, and ESRF Grenoble for support and discussion during EXAFS analysis session, Justin Hamilton and Jim Sharp, University of Surrey, for characterizing some samples by Hall Effect measurements. They acknowledge the support of the European Commission under the action "Structuring the European Research Area." Portions of this research were carried out at the Stanford Synchrotron Radiation Lightsource, a national user facility operated by Stanford University on behalf of the U.S. Department of Energy, Office of Basic Energy Sciences. The work of M.A.S. is supported by Research Corporation Award No. CC6405 and NSF Grant No. DMI 0420952.

[1]R. Duffy, T. Dao, Y. Tamminga, K. van der Tak, F. Roozeboom, and E. Augendre, Appl. Phys. Lett. **89**, 071915 (2006).
[2]A. Lietoila, J. F. Gibbons, T. J. Magee, J. Peng, and J. D. Hong, Appl. Phys. Lett. **35**, 532 (1979).
[3]D. Nobili, S. Solmi, A. Parisini, M. Derdour, A. Armigliato, and L. Moro, Phys. Rev. B **49**, 2477 (1994).
[4]P. M. Rousseau, P. B. Griffin, W. T. Fang, and J. D. Plummer, J. Appl. Phys. **84**, 3593 (1998).
[5]J. L. Allain, J. R. Regnard, A. Bourret, A. Parisini, A. Armigliato, G. Tourillon, and S. Pizzini, Phys. Rev. B **46**, 9434 (1992).
[6]O. Dokumaci, P. M. Rousseau, S. Luning, V. Krishnamoorthy, K. S. Jones, and M. E. Law, J. Appl. Phys. **78**, 828 (1995).
[7]K. Saarinen, J. Nissila, H. Kauppinen, M. Hakala, M. J. Puska, P. Hautojarvi, and C. Corbel, Phys. Rev. Lett. **82**, 1883 (1999).
[8]M. Ramamoorthy and S. T. Pantelides, Phys. Rev. Lett. **76**, 4753 (1996).
[9]D. C. Mueller, E. Alonso, and W. Fichtner, Phys. Rev. B **68**, 045208 (2003).
[10]S. A. Harrison, T. F. Edgar, and G. S. Hwang, Phys. Rev. B **74**, 195202 (2006).
[11]N. Kong, S. K. Banerjee, T. A. Kirichenko, S. G. H. Anderson, and M. C. Foisy, Appl. Phys. Lett. **90**, 062107 (2007).
[12]D. Giubertoni *et al.*, J. Appl. Phys. **104**, 103716 (2008).
[13]D. Giubertoni, M. Bersani, M. Barozzi, S. Pederzoli, E. Iacob, J. A. van den Berg, and M. Werner, Appl. Surf. Sci. **252**, 7214 (2006).
[14]D. Giubertoni *et al.*, AIP Conf. Proc. **1173**, 45 (2009).
[15]D. Giubertoni, G. Pepponi, M. Bersani, S. Gennaro, F. D'Acapito, R. Doherty, and M. A. Foad, Nucl. Instrum. Methods Phys. Res. B **253**, 9 (2006).
[16]F. Iacona, V. Raineri, F. La Via, A. Terrasi, and E. Rimini, Phys. Rev. B **58**, 10990 (1998).